Research Fund, administered by the American Chemical Society, the Air Force Office of Scientific Research (Grant No. 82-0190), and the North Dakota State University Computer Center.

Registry No. SiH_2, 13825-90-6; NH_3, 7664-41-7; H_2O, 7732-18-5; HF, 7664-39-3; PH_3, 7803-51-2; H_2S, 7783-06-4; HCl, 7647-01-0.

Supplementary Material Available: Listing of complete 6-31G* geometry specifications (7 pages). Ordering information is given on any current masthead page.

Experimental Determination of the Bond Density of Molecular Hydrogen in Momentum-Space by Binary (e,2e) Spectroscopy

K. T. Leung and C. E. Brion*

Contribution from the Department of Chemistry, The University of British Columbia, Vancouver, British Columbia, Canada V6T 1Y6. *Received October 3, 1983*

Abstract: The spherically averaged bond density of molecular hydrogen in momentum-space has been derived by using the momentum distribution of the H_2 $1\sigma_g$ orbital determined by binary (e,2e) spectroscopy and the exact solution of the Schrodinger equation for the 1s orbital of the H atom. Theoretical bond densities calculated by using different quality wave functions ranging from minimal basis set to extended Hartree–Fock are given for comparison. In addition, the orbital momentum moments of the H_2 $1\sigma_g$ orbital are estimated from the measured orbital momentum distribution (Leung, K. T.; Brion, C. E. *Chem. Phys.* **1983**, *82*, 113.) and are found to be in good agreement with those calculated by using theoretical wave functions. Moreover, the dependence of the bond density on the quality of the wave function is discussed by using density difference maps in both position and momentum-space. The formation of the σ bond in momentum-space is also examined topographically in the critical range of internuclear separation between 2 and 1 a_0. The bonding picture in momentum-space complements traditional position-space bonding concepts and further extends present understanding of momentum-space chemistry.

I. Introduction

The ground-state electronic wave function of molecular hydrogen has been the subject of many experimental investigations including binary (e,2e) spectroscopy[1,2] and Compton scattering.[3] Compton scattering experiments in general sample the momentum density due to all the electrons of the target. Binary (e,2e) spectroscopy[4] on the other hand, samples selectively the momentum density of individual orbitals and provides a direct and sensitive experimental evaluation of molecular orbital wave functions. In the case of H_2, the total momentum density is to a very good approximation that of the $1\sigma_g$ orbital. The generally good agreement of the momentum distribution of molecular hydrogen observed by the two different techniques has been demonstrated in our recent study using binary (e,2e) spectroscopy.[2] The ground-state wave function of H_2 has also been investigated by many elaborate theoretical ab initio calculations, and H_2 is also the simplest test molecule for configurational interaction methods. Moreover, the hydrogen molecule involves the simplest (covalent) chemical bond and is thus suitable for the most fundamental studies of chemical binding and electronic structural properties. Earlier works by Berlin,[5] Roux et al.,[6] and Bader et al.[7,8] involved position (charge) density difference (bond density) maps and the force concept. Other works by Bader and Preston[9] and by Feinberg et al.[10,11] examined the behavior of the kinetic and potential energy upon bond formation and the role of the Virial theorem in bond formation.

The bond density in either position or momentum space is defined in the present study to be the density difference between the molecular density ($\rho_{H_2 1\sigma_g}$) and the density due to independent atoms (the independent atom model density, ρ_{IAM}) at positions corresponding to the molecular nuclear geometry, i.e.

$$\Delta\rho = 2\rho_{H_2 1\sigma_g} - \rho_{IAM} \quad (1a)$$

$$\rho_{IAM} = \rho_{H1s} + \rho_{H1s} \quad (1b)$$

both at R, where R is the internuclear separation and ρ denotes the single electron density. It is possible to obtain the "experimental" (spherically averaged) momentum-space bond density using the experimental momentum distributions of the H_2 $1\sigma_g$ orbital and either the experimental or the exact theoretical momentum distribution of the 1s orbital for the H atom. The momentum distribution for the 1s orbital of atomic hydrogen has been determined recently in an elegant experiment by Lohmann and Weigold[12] using binary (e,2e) spectroscopy. The measured result is found to reproduce the square of the exact solution of the Schrodinger equation in momentum-space. The only difficulty involved in obtaining the bond density is the normalization of the measured spherically averaged momentum density of H_2 $1\sigma_g$ because the noncoplanar symmetric (e,2e) experiment in most cases measures only relative cross sections.[4] In the present study, this problem is solved by employing a numerical procedure. The "experimental" momentum-space bond density thus obtained is compared with theoretical calculations by using H_2 wave functions of different quality including extended Hartree–Fock (Ext-HF),[13]

(1) Weigold, E.; McCarthy, I. E.; Dixon, A. J.; Dey, S. *Chem. Phys. Lett.* **1977**, *47*, 209.
(2) Leung, K. T.; Brion, C. E. *Chem. Phys.* **1983**, *82*, 113.
(3) Lee, J. S. *J. Chem. Phys.* **1977**, *66*, 4906.
(4) McCarthy, I. E.; Weigold, E. *Phys. Rep.* **1976**, *27C*, 276.
(5) Berlin, T. J. *Chem. Phys.* **1951**, *19*, 208.
(6) Roux, M.; Cornille, M. J. *Chem. Phys.* **1962**, *37*, 933.
(7) Bader, R. F. W.; Henneker, W. H. *J. Chem. Phys.* **1967**, *46*, 3341.
(8) Bader, R. F. W.; Chandra, A. K. *Can. J. Chem.* **1968**, *46*, 953.
(9) Bader, R. F. W.; Preston, H. J. T. *Int. J. Quantum Chem.* **1969**, *3*, 327.
(10) Feinberg, M. J.; Ruedenberg, K.; Mehler, E. L. *Adv. Quantum Chem.* **1970**, *5*, 28.
(11) Feinberg, M. J.; Ruedenberg, K. *J. Chem. Phys.* **1971**, *54*, 1495.
(12) Lohmann, B.; Weigold, E. *Phys. Lett.* **1981**, *86A*, 139.

0002-7863/84/1506-5859$01.50/0

Table I. Orbital Momentum Moments of H_2 $1\sigma_g$ Orbital (au)

	experimetnal[a]			theory[b]				
moment	OLDF	BSZ	TTP	Ext-HF	Ltd-HF	DZ	MBS	Lee[c]
$\langle p^2 \rangle$	6.36	7.56	7.62	8.24	7.86	7.20	6.92	8.32 (0.25)
$\langle p^1 \rangle$	2.62	2.96	2.96	3.18	3.02	3.02	2.96	3.08 (0.02)
$\langle p^0 \rangle$	2.00	2.00	2.00	2.00	2.00	2.00	2.00	1.99 (0.02)
$\langle p^{-1} \rangle$	2.46	1.96	1.92	1.82	1.82	1.84	1.90	1.86 (0.02)
$\langle p^{-2} \rangle$	2.86	2.62	2.50	2.26	2.26	2.26	2.40	2.34 (0.09)

[a] The accuracy is expected to be about ±7%. [b] The accuracy is about ±4%. Note that the various wave functions are Ext-HF,[13] Ltd-HF,[14] DZ,[15] and MBS.[16] [c] The moments are evaluated by Lee[3] by using a similar two-term polynomial optimization of the Compton scattering data. Uncertainties are shown in parentheses.

limited Hartree–Fock (Ltd-HF),[14] double-zeta (DZ),[15] and minimal basis set (MBS).[16] In addition, the dependence of the bond density on the quality of the wave function is also examined by directional momentum-space and position-space density difference maps.[2,5-9,17-20] Earlier studies[2] of the bonding in H_2 at large step spacings between internuclear separations of $R = 8$ and 1 a_0 have indicated that dramatic changes in momentum-space bond density occur between $R = 2$ and 1 a_0. Therefore, we have now extended the topographical study of the momentum-space bond density in H_2 to explore in detail the critical range of R = 2–1 a_0 using the extended Hartree–Fock quality wave function of Das and Wahl.[13] The present study provides a complementary look at chemical bonding phenomena of H_2 in momentum and position space and further illustrates momentum-space chemical concepts.[2,17,18,21-23] A three-dimensional representation is shown for the H_2 $1\sigma_g$ single covalent bond in momentum-space.

II. Estimation of the Orbital Moments and Normalization of the Momentum Distribution

Binary (e,2e) spectroscopy has been discussed in considerable detail in earlier publications.[4,22-24] In brief, the method measures the binding energy spectra and momentum distributions of electrons in individual orbitals by using high-energy electron impact and coincident detection of the two outgoing electrons. The measured cross sections are usually interpreted by using the plane wave impulse and target Hartree–Fock approximations, in which case the measured cross section can be shown to be proportional to the spherically averaged momentum density of the jth orbital, $\{\rho_j(p)\}$.[4] The momentum distributions are spherically averaged due to the random orientation of the gaseous targets. In practice, only relative cross sections are determined in binary (e,2e) experiments. In the present work, the spherically averaged momentum-space bond density of H_2 $1\sigma_g$ is obtained by eq 1 by using the experimentally determined momentum distribution[2] of the H_2 $1\sigma_g$ orbital (appropriately normalized) and the exact atomic hydrogen 1s momentum distribution.[12] The experimental momentum distribution of the H 1s orbital has been shown to be in excellent agreement with the exact solution (squared) of the Schrodinger equation in momentum-space.[12] The procedure for normalization of the relative spherically averaged momentum

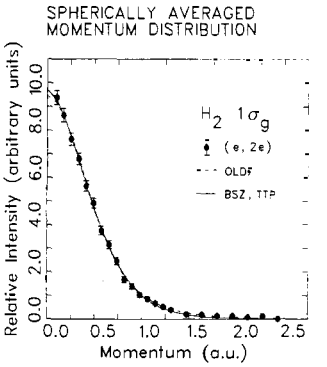

Figure 1. Comparison of the spherically averaged experimental momentum distribution of the H_2 $1\sigma_g$ orbital with the fitted semiempirical density functions: OLDF, BSZ, TTP. The BSZ and TTP functions are indistinguishable from each other.

density of the H_2 $1\sigma_g$ orbital to give an absolute density is outlined below. Briefly, an analytical function is fitted to the experimental spherically averaged momentum distribution by using a square residual minimization method.[25,26] The nth-order momentum moments of the jth orbital, $\langle p^n \rangle_j$, are then evaluated from the fitted function by using standard numerical integration techniques.[25]

$$\langle p^n \rangle_j = 4\pi \int \{\rho_j(p)\} p^{n+2} dp \qquad (2a)$$

where $\{\rho_j(p)\}$ is the spherically averaged momentum distribution of the jth orbital. The experimental distribution and the optimized analytical density function can be normalized by the zeroth-order moment. In the case of H_2, we have

$$\langle p^0 \rangle_{1\sigma_g} = \text{occupancy number of } 1\sigma_g \text{ orbital} = 2 \qquad (2b)$$

Three semiempirical analytical functions are used to approximate $\{\rho(p)\}$ of the H_2 $1\sigma_g$ orbital. These are:

(i) orbital local density functional (OLDF) density

$$\{\rho(p)\} = K(p^2/2 + a_1 p + a_2)^{-3}$$

(ii) best single-zeta (BSZ) density

$$\{\rho(p)\} = K(\zeta^5)(\zeta^2 + p^2)^{-4}$$

(iii) two-term polynomial (TTP) density

$$\{\rho(p)\} = K_1(\gamma_1^2 + p^2)^{-4} + K_2(\gamma_2^2 + p^2)^{-5}$$

The linear parameters, K's, are normalization constants. Both the linear (K's) and the nonlinear parameters (a's, ζ's, and γ's) are optimized by fitting to the experimental momentum distribution in the numerical procedure.[26] The OLDF density form used here is that given by Pathak et al.[27] and should strictly be used for the total momentum density of atoms in the local density functional approximation.[28] The BSZ (best single-zeta) mo-

(13) Das, G.; Wahl, A. C. *J. Chem. Phys.* **1966**, *44*, 87.
(14) Fraga, S.; Ransil, B. J. *J. Chem. Phys.* **1961**, *35*, 1967.
(15) Snyder, L. C.; Basch, H. "Molecular Wave Functions and Properties"; Wiley: New York, 1972.
(16) The minimal basis set used is the standard STO-3G basis in the GAUSSIAN 76 package. See, for example: Hehre, W. J.; Lathan, W. A.; Ditchfield, R.; Newton, M. D.; Pople, J. A. "National Resource Computer Software Catalog"; 1980; Vol. 1, GAUSSIAN 76.
(17) Coulson, C. A.; Duncanson, W. E. *Proc. Cambridge Philos. Soc.* **1941**, *37*, 55, 67, 74, 397, 406; **1942**, *38*, 100; **1943**, *39*, 180.
(18) Epstein, I. R.; Tanner, A. C. "Compton Scattering"; Williams, B. G., Ed.; McGraw-Hill: New York, 1977, pp 209.
(19) Henneker, W. H.; Cade, P. E. *Chem. Phys. Lett.* **1968**, *2*, 575.
(20) Ramirez, B. I. *Chem. Phys. Lett.* **1983**, *94*, 180.
(21) Cook, J. P. D.; Brion, C. E. "Momentum Wave Functions-1982"; Weigold, E., Ed.; American Institute of Physics: New York, 1982; American Institute of Physics Conference Proceedings, No. 86, pp 278.
(22) Camilloni, R.; Stefani, G.; Fantoni, R.; Giardini-Guidoni, A. *J. Electron Spectrosc. Relat. Phenom.* **1979**, *17*, 209.
(23) Moore, J. H.; Tossell, J. A.; Coplan, M. A. *Acc. Chem. Res.* **1982**, *15*, 195.
(24) Leung, K. T.; Brion, C. E. *Chem. Phys.* **1983**, *82*, 87.
(25) Lootsma, F. "Numerical Methods for Non-Linear Optimization"; Academic Press: New York, 1972.
(26) Moore, C. "Curve Fitting Routines"; The University of British Columbia, Computing Centre: September 1981; UBC CURVE.
(27) Pathak, R. K.; Panat, P. V.; Gadre, S. R. *Phys. Rev.* **1982**, *A26*, 3073.
(28) Levy, M. *Proc. Natl. Acad. Sci. U.S.A.* **1979**, *76*, 6062.

mentum density corresponds to the square of the Fourier transform of a position-space 1s Slater-type orbital[29] with the ζ value optimized to give the best fit to the experimental momentum distribution. The two-term polynomial function (TTP) is used by Lee[3] in his study of the total momentum density of H_2 by high-energy electron impact spectroscopy. It should be noted that the two-term polynomial function is essentially the BSZ function with an additional high-order term.

Figure 1 shows the experimental momentum distribution of the H_2 $1\sigma_g$ orbital obtained recently by a high-momentum resolution binary (e,2e) spectrometer[2,24] along with the fitted analytical density functions. It is obvious that all three semiempirical density functions give an excellent fit to the experimental data. The BSZ and TTP densities are indistinguishable from each other while the OLDF density is only slightly different from the BSZ and TTP densities in the low- and high-momentum region.

Table I shows the orbital momentum moments calculated by using the optimized density functions. Orbital moments evaluated directly from ab initio SCF wave functions of different quality[13-16] are also given. These moments are compared with those reported by Lee.[3] Clearly, there is an overall good agreement between the "experimental" orbital moments (less good for the higher moments $\langle p^2 \rangle$) and the theoretical ones. The semiempirical BSZ and TTP moments are quite close to each other with the OLDF moments being noticeably different. In particular, the OLDF density significantly underestimates the average orbital moment ($\langle p \rangle$). This deficiency is due to the form of the OLDF density, which in general will lead to a broader total momentum distribution even for atoms.[27] The OLDF moments show that the reported form of the OLDF function[27] is not adequate to represent the momentum density of small molecules like hydrogen. It is also evident from Table I that the "experimental" moments are slightly different from the theoretical ones. The estimated averaged orbital momenta ($\langle p \rangle$) are generally slightly lower than the theoretical ones. This suggests that the H_2 $1\sigma_g$ orbital is actually less spatially diffuse (in position-space) than that predicted by the more sophisticated ab initio wave functions. It should be noted that the momentum distribution measured at a particular binding energy is in general related to the overlap form factor.[4] In the target Hartree–Fock approximation,[4] the form factor can be simplified to the orbital momentum density. It is also possible that small differences in the estimated orbital momenta ($\langle p \rangle$) between the experiment and theories may be attributed to the inadequacy of the target Hartree–Fock approximation. The results of binary (e,2e) spectroscopy involve vibrational averaging over the final ion state.[4] The effects of this averaging on the comparison of experimentally determined momentum distributions and those calculated at a single R value are expected to be negligible as demonstrated by the work of Dey et al.[30] on H_2 and D_2.

III. Spherically Averaged Momentum-Space Bond Density

Figure 2 shows the spherically averaged momentum-space bond density of H_2. The right-hand section of Figure 2 shows the detail between 0.5 and 1.5 a_0^{-1}. The constants optimized in the orbital moment estimation procedure are used to normalize the experimental spherically averaged momentum distribution of the H_2 $1\sigma_g$ orbital.[2] The independent atom model density is obtained from the exact solution for the H 1s orbital. Equation 1 is then used to calculate the bond density. Theoretical bond densities corresponding to different quality wave functions of the H_2 $1\sigma_g$ orbital are also given for comparison.

Several interesting features are apparent. First, the spherically averaged momentum-space (p space) bond density consists of a negative well and a positive wing tailing off to $p = \infty$ with the zero crossing point at $p \simeq 0.8$ a_0^{-1}. Although the directional information is lost after the spherical averaging, one can see that a σ bond is characterized by a transfer of momentum density (fractional current) from the low-momentum region to the high-momentum region. In addition, the variationally less superior

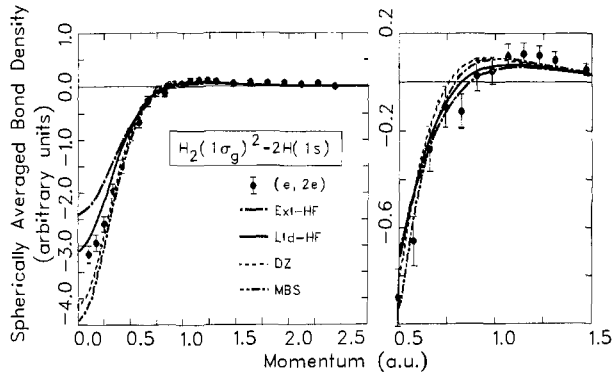

Figure 2. Spherically averaged momentum space bond density of H_2. Theoretical bond densities are evaluated by using H_2 $1\sigma_g$ wave functions of different quality ranging between extended Hartree–Fock (Ext-HF),[13] limited Hartree–Fock (Ltd-HF),[14] double-zeta (DZ),[15] and minimal basis set (MBS).[16] The wave function for atomic H is the exact solution of the Schrodinger equation.[10] An exploded view of the bond density in the range 0.5–1.5 a_0^{-1} is given to illustrate the positive "wing" of the bond density.

DZ[15] and MBS[16] wave functions have "deeper wells" (i.e., more negative minima) at the p-space origin and slightly sharper "wings" (positive maxima) than the more sophisticated ones.[13,14] Furthermore, the "experimental" bond density lies between the limited Hartree–Fock and the double-zeta quality bond densities at low momentum. It is, however, in closer agreement with the limited Hartree–Fock curve near the momentum origin. It should be noted[2] that the experimental spherically averaged momentum distribution of the H_2 $1\sigma_g$ orbital gives generally good agreement with theoretical density functions calculated by using the limited Hartree–Fock and better quality wave functions. The momentum-space bond density shows the differences between different wave functions more clearly than the straightforward comparison of the momentum distributions (see Figure 5b of ref 2). The momentum-space bond density is therefore an alternative way to evaluate wave functions by comparing with experimental (e,2e) data, at least in the special case of the hydrogen molecule where the bond density can readily be derived.

IV. Directional Bond Density

1. Wave Function Dependence. Except where otherwise stated, the density contour values of the directional bond density (density difference) maps used throughout the present study correspond to 80, 60, 40, 20, ±8, ±6, ±4, ±2, ±0.8, and ±0.6% of the absolute maximum density difference value. Contours of negative density difference are shown as dashed lines. The directions of the cutting plane are defined by two vectors, i.e., the bond-parallel or internuclear (0,0,1) vector and the bond-perpendicular (0,1,0) vector. The projection plots on the right-hand side and on the top of the contour maps show the relative change in magnitude of the bond density function along and perpendicular to the internuclear axis (dotted lines), respectively. The position and momentum are in atomic units.

Figure 3 shows the directional density difference maps corresponding to H_2 $1\sigma_g$ wave functions of different quality ranging between extended Hartree–Fock (Ext-HF),[13] limited Hartree–Fock (Ltd-HF),[14] double-zeta (DZ),[15] and minimal basis set (MBS).[16] The equilibrium internuclear separation (1.4 a_0) has been used for the calculations shown in Figure 3. It should be noted that because of the nature of the DZ and MBS wave functions, the contour values for the momentum-space (p space) bond density (density difference) maps have been extended to include ±0.4, ±0.2, −0.08, −0.06, −0.04, and −0.02% of the *absolute* maximum density difference value.

It is evident that all four wave functions provide a qualitatively similar picture for the σ bond. In general, the σ bond in H_2 in position-space (r-space) can be associated with the familiar "hamburger" picture, namely, density (fractional charge) accumulation in the internuclear region and density depletion at the end regions of the molecule.[8] In momentum-space (p-space) a

(29) Komarov, F. F.; Temkin, M. M. *J. Phys. B*: **1976**, *9*, L255.
(30) Dey, S.; McCarthy, I. E.; Teubner, P. J. O.; Weigold, E. *Phys. Rev. Lett.* **1975**, *34*, 782.

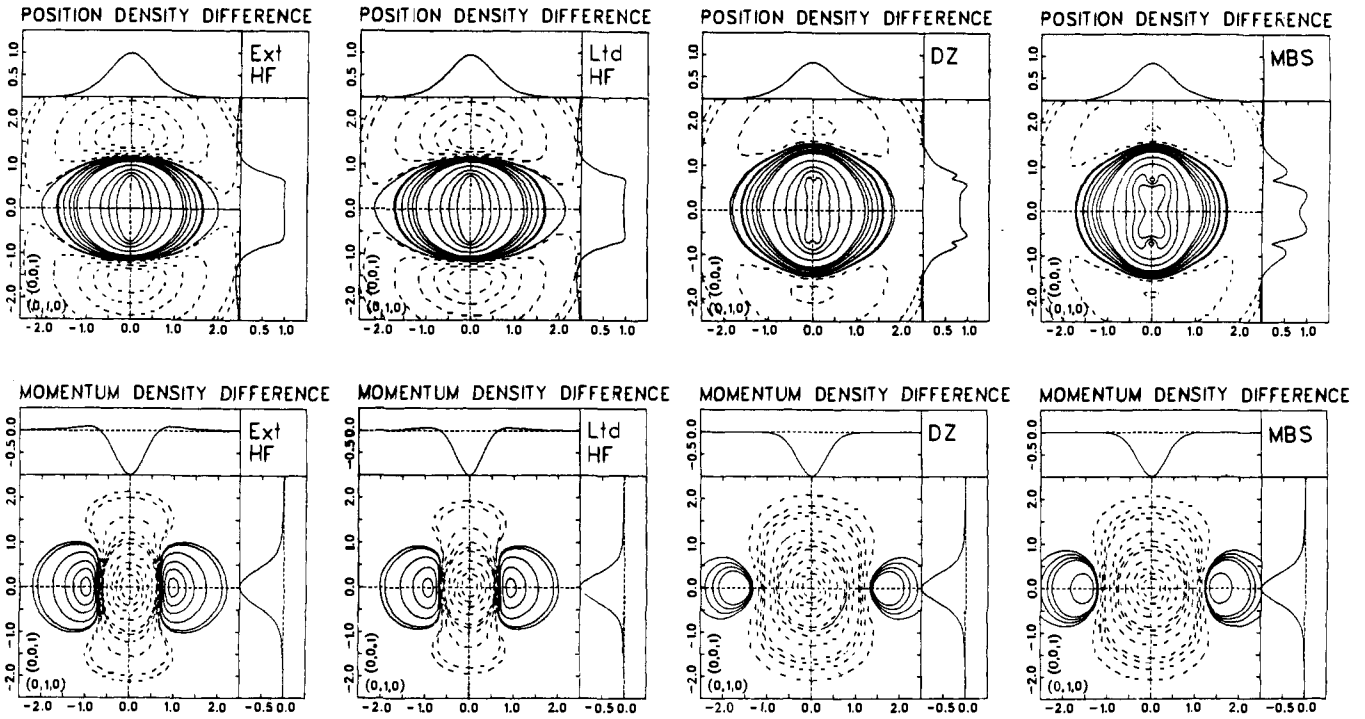

Figure 3. Directional density difference (bond density) maps in momentum and position space as a function of the type of H_2 $1\sigma_g$ wave function. The extended Hartree–Fock (Ext-HF),[13] limited Hartree–Fock (Ltd-HF),[14] double-zeta (DZ),[15] and minimal basis set (MBS)[16] wave functions at the equilibrium internuclear separation (1.4 a_0) are used. The contour values are +80, +60, +40, +20, ±8, ±6, ±4, ±2, ±0.8, and ±0.6% of the maximum absolute density difference values. For the DZ and MBS bond densities, additional contours at ±0.4, ±0.2, −0.08, −0.06, −0.04, and −0.02% of the maximum absolute density difference values are included. Contours of negative density difference are shown as dashed lines. The position and momentum are in atomic units. The internuclear (bond parallel) direction is along the (0,0,1) vector.

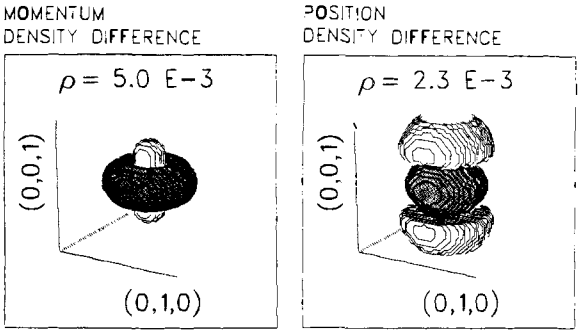

Figure 4. Three-dimensional surface plot of the density difference (bond density) of H_2 in momentum and position space. The extended Hartree–Fock[13] wave function at equilibrium internuclear geometry is used to generate the bond density surfaces. The bond density surfaces correspond to ±2% of the maximum bond density values in the respective spaces. Positive bond density surfaces are shaded.

complementary view of the σ bond is obtained as discussed in our earlier work.[2] In this "bone in a donut" (or torus) model,[2] momentum density (fractional current) is depleted through the p-space origin along the internuclear direction (the "bone" part) and is localized annularly in the high-momentum bond-perpendicular region (the "donut"). Similar ideas have also recently been presented by Ramirez.[20] It should be noted that the cylindrical symmetry of the σ bond in r-space is preserved in p-space. This is, of course, a direct consequence of the Fourier transform properties discussed previously.[2,18] A three-dimensional surface plot of the bond densities generated by using the Ext-HF wave function[13] is shown in Figure 4 to better visualize the nature of the H_2 $1\sigma_g$ bond in both p- and r-space. The bond densities for surfaces shown correspond to ±2% of the maximum bond density values in the respective spaces.

Although all four wave functions show the same general density topographical features (see Figure 3), there are some important differences, especially between Ltd-HF and DZ. For the Ext-HF and Ltd-HF bond densities both the r-space and p-space bond densities, respectively, appear to be quite similar. The only noticeable difference is in the end regions of the "bone" part. The major difference occurs between the Ltd-HF and the DZ bond densities. The pronounced change in the nature of the wave function can be seen in the r-space bond density whereby the bond-perpendicular ellipsoidal positive lobe of the Ltd-HF (and Ext-HF) becomes more spherical in the DZ (and MBS). This can be seen more clearly in the bond-parallel projection plots, which show the appearance of four well-defined positive maxima for the DZ (and MBS) instead of the flat positive "plateau" for the Ltd-HF (and Ext-HF). The negative lobe of the DZ not only has a relatively smaller amplitude but also is further away from the r-space origin. Even more dramatic differences can be seen in the p-space density difference maps. (Note that more contour lines with smaller bond density values are included for the DZ and MBS bond densities in Figure 3). The p-space bond of the DZ (and also MBS) is dominated by the negative "bone" structure, which appears also to be considerably broader than that of the Ltd-HF (and Ext-HF) one. The positive "donut" structure can only be seen when relative contour values below 0.1% of the maximum amplitude are used. In the case of the MBS wave function, its r-space bonding structure is even more inadequate as shown by the bond-parallel projection plot. The p-space "donut" structure is also slightly larger compared to the DZ one.

2. Dependence of Internuclear Separation. Figure 5 shows the directional bond density (density difference) in both p-space and r-space corresponding to the extended Hartree–Fock quality wave function of Das and Wahl[13] as a function of internuclear separation, R. Earlier work by Bader and Chandra[8] reported the r-space bond density maps evaluated by using the same Ext-HF wave function[13] as a function of R. The present work studies the progress of bond formation in p-space over the critical separation range of $1.0\ a_0 \leq R \leq 2.0\ a_0$. A preliminary study of bond formation over a more extensive range and wider spacing of selected R values has been given earlier.[2] It should be noted that comparison can only be made within a single difference map since contour values are relative to the maximum bond density. The maximum bond densities in the contour planes are shown in Table

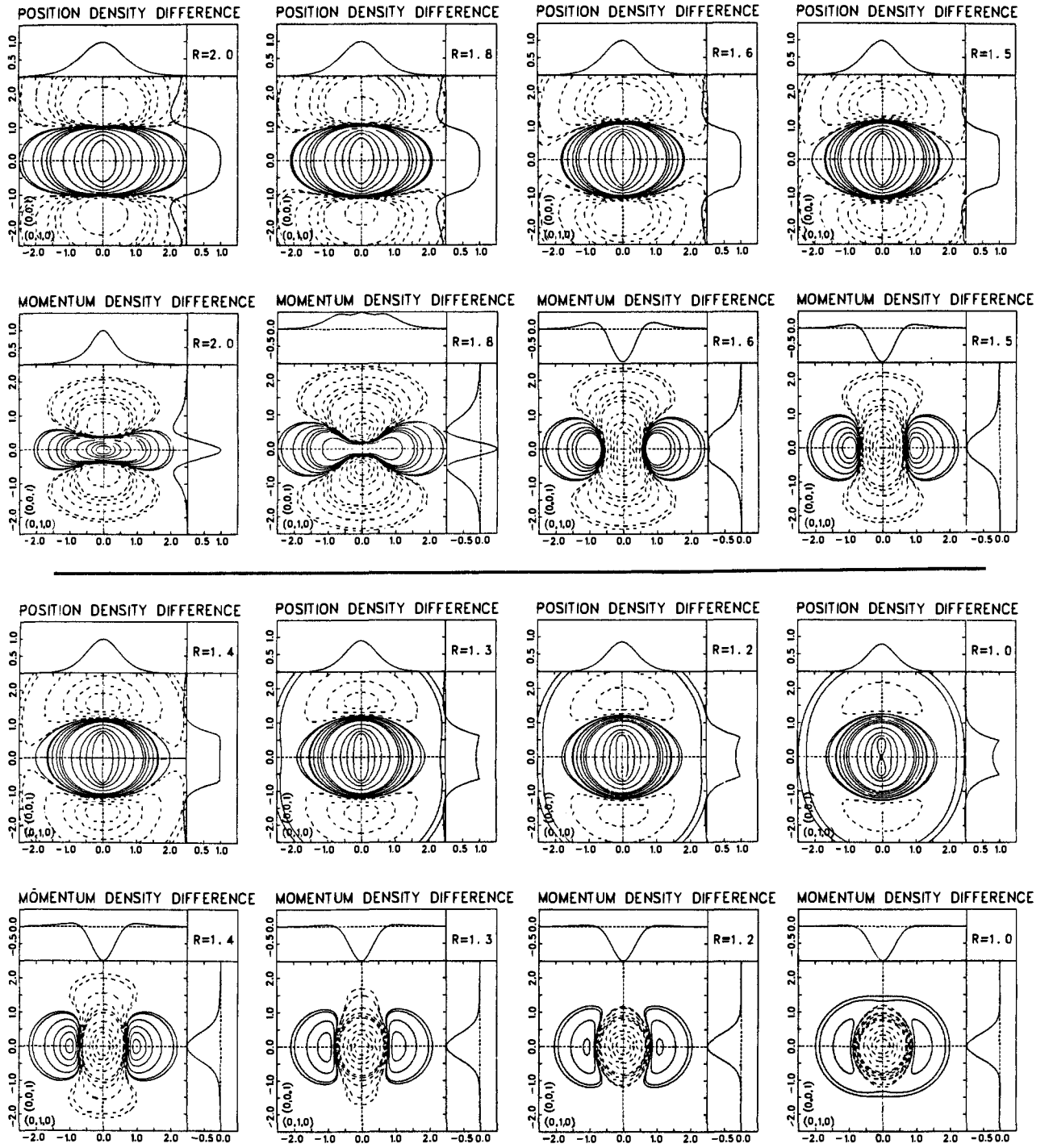

Figure 5. Directional density difference (bond density) maps in momentum and position space as a function of internuclear separation R. The extended Hartree–Fock[13] wave functions at the corresponding R are used to generate the maps. The contour values are +80, +60, +40, +20, ±8, ±6, ±4, ±2, ±0.8, and ±0.6% of the maximum absolute density difference values (see Table II). Contours of negative density difference are shown as dashed lines. The position and momentum are in atomic units. The internuclear (bond parallel) direction is along the (0,0,1) vector.

II to give some indication of the global change as the H atoms approach each other.

Bond formation as represented by this series of σ bond density maps for H_2 involves the transfer of density from the antibinding region to the binding region. The r-space binding region is, of course, the small r (i.e., internuclear) region with density extended preferentially in the bond-perpendicular direction while the antibinding region is at large r outside the nuclei extending preferentially in the bond-parallel direction.[2] In contrast, the locations of the binding and antibinding regions in p-space are reversed. Specifically, the binding region in p-space is the annular (bond-perpendicular) high p region while the antibinding region is centered at low p and distributed preferentially along the bond-parallel direction. Between $R = 2.0\ a_0$ and the equilibrium separation at $1.4\ a_0$, the gradual charge accumulation in the r-space binding region is particularly obvious as shown in the bond-parallel projection plots. Further closer approach of the H atoms causes charge saturation in the internuclear region, causing the pileup of density at the maxima seen particularly clearly at $R = 1.0\ a_0$. A much more dramatic change can be seen in the p-space density difference. At $R = 2.0\ a_0$ the p-space bond density is in fact somewhat similar in shape to its r-space counterpart. In the R range of 2.0–1.4 a_0, the penetration of the negative lobe of the p-space bond density into the positive lobe along the bond axis results in the formation of the binding "donut" structure. This dramatic change (in marked contrast to the r-space pictures which only change marginally) is remarkably obvious in both the bond-parallel and the bond-perpendicular projection plots. Most

Table II. Maximum Absolute Values of Bond Density as a Function of R[a]

R	maximum bond density	
	r space	p space
2.0	0.0451	0.192
1.8	0.0593	-0.0769
1.6	0.0792	-0.122
1.5	0.0930	-0.197
1.4	0.113	-0.276
1.3	0.142	-0.354
1.2	0.178	-0.433
1.0	0.281	-0.585

[a] R and the bond density are in atomic units. Note that the equilibrium internuclear separation is 1.4 a_0.

notable is the change between R = 1.8 and 1.6 a_0. Below the equilibrium internuclear distance (1.4 a_0) closer approach of the H atoms results in the transfer of momentum density back into the antibinding bond-parallel high p region. The enclosure of the negative lobe by the positive lobe generates the unstable oval structure at R = 1.0 a_0.

The difference in density relocation in r-space and p-space is in accord with the Virial property.[2,18] The formation of a stable system must be accompanied by the lowering of the total energy or equivalently by the raising of the kinetic energy. The kinetic energy (T) can be increased more effectively by transferring the density into the high-momentum bond-perpendicular region because the parallel component ($T_\parallel$) of the kinetic energy of a diatomic is smaller than the perpendicular component ($T_\perp$).[9-11] The phenomenological change in p-space bond density upon bond formation is indicative of this Virial requirement.[2] In this regard, Bader and Preston[9] have shown earlier that the difference between the bond-perpendicular and bond-parallel components of the kinetic energy, $(T_\perp - T_\parallel)/T$, reaches its maximum in H_2 between R = 2.0 and 1.4 a_0. The results of the present investigations are entirely consistent with the theoretical analysis of kinetic energy density in H_2 given by Bader and Preston.[9] The presently reported experimental studies of the distribution of bond density in momentum space are also consistent with the predictions made in the pioneering theoretical work of Coulson and Duncanson[17] in 1941 concerning the electron momentum distribution in a single bond. Finally, the p-space bond density maps complement the r-space bond density maps to provide a more complete bonding picture. Namely, the formation of a stable σ bond in molecular hydrogen can be regarded as a transformation of the "slow" charge moving with a low momentum along the bond axis at the ends of the molecule to "fast" charge moving with a high momentum perpendicular to the bond axis in the internuclear space of the molecule. Clearly bond formation is manifested, in the present study, much more dramatically in momentum-space than in position-space. Since measurements are possible in p-space but thus far not in r-space, the use of momentum-space concepts and binary (e,2e) spectroscopy promises new vistas of chemical bonding in both experimental and theoretical work.

Acknowledgment. Financial support for this work was provided by the Natural Sciences and Engineering Research Council (NSERC) of Canada. K. T. Leung gratefully acknowledges the receipt of an NSERC postgraduate scholarship.

Registry No. Hydrogen, 1333-74-0.

Correlation Effects and Bond-Correlation Energies in the Series of Molecules Including C_1 to C_4 Hydrocarbons. Fourth-Order MB-RSPT Calculations

V. Kellö,*† M. Urban,† J. Noga,† and G. H. F. Diercksen‡

Contribution from the Department of Physical Chemistry, Faculty of Science, Comenius University, Mlynská dolina, 842 15 Bratislava, Czechoslovakia, and Max-Planck-Institut für Physik und Astrophysik, Institut für Astrophysik, D-8046 Garching bei München, Federal Republic of Germany. *Received August 15, 1983*

Abstract: The MB-RSPT up to the fourth order was applied to the calculations of the correlation energies in the series of molecules (including C_1 to C_4 hydrocarbons and the oxygen-containing molecules) using the Gaussian DZ+P basis set. We analyzed the correlation effects which arise from individual types of excitations (single, double, triple, and quadruple) as a function of the number of electrons and the bonding situation in the molecule. The lowest value of the correlation energy per electron pair was found from a series of C_1 to C_3 alkanes. The correlation energy increases in molecules with a double C=C bond, oxygen-containing single bond, adjacent double C=C bonds (CH_2CCCH_2), and triple C≡C bonds and is highest in molecules with multiple carbon–oxygen bonds adjacent to another multiple bond (CH_2CCO). We also present the bond-correlation energies and examine the additivity of the bond-correlation contributions.

Attempts to estimate the correlation energy in large molecules already have a rather long history. The simplest conceivable approach is based on the assumption of a constant value of the correlation energy for each type of bonding in the molecules.[1-6] Using the principle of additivity (or implicitly the linear dependence of an appropriate type) the correlation energy is given as a sum of these bond contributions. Although this method cannot be applied in all problems where the correlation effects are important, it may be useful at least in one important topic, namely in estimation of reaction energies.

The naive principle of additivity is not new. In the present context it has been used for a long time in thermodynamics (see,

† Comenius University.
‡ Max-Planck-Institut.

(1) Snyder, L. C.; Basch, H. *J. Am. Chem. Soc.* **1969**, *91*, 2189.
(2) Hollister, C.; Sinanoglu, O. *J. Am. Chem. Soc.* **1966**, *88*, 13.
(3) George, P.; Trachtman, M.; Brett, A. M.; Bock, C. W. *Int. J. Quantum Chem.* **1977**, *12*, 61.
(4) Moffat, J. B. *J. Mol. Struct.* **1973**, *15*, 325.
(5) Pople, J. A.; Binkley, J. S. *Mol. Phys.* **1975**, *29*, 599.
(6) Cremer, D. *J. Comput. Chem.* **1982**, *3*, 165.

0002-7863/84/1506-5864$01.50/0